IODP Expedition 333: Return to Nankai Trough Subduction Inputs Sites and Coring of Mass Transport Deposits

by Pierre Henry, Toshiya Kanamatsu, Kyaw Thu Moe, Michael Strasser, and the IODP Expedition 333 Scientific Party

Abstract

Integrated Ocean Drilling Program (IODP) Expedition 333 returned to two sites drilled during IODP Expedition 322 on the ocean side of the Nankai Trough to pursue the characterization of the inputs to the Nankai subduction and seismogenic zone, as part of the Nankai Trough Seismogenic Experiment (NanTroSEIZE) multi-expedition project. Site C0011 is located at the seaward edge of the trench and Site C0012 on a basement high, Kashinozaki Knoll (Fig. 1). The main objectives of drilling again at these sites were to fill coring gaps in the upper part (<350 m) of the sedimentary sequence, to measure heat flow, and to core the oceanic base-ment to a greater depth on the Knoll. New results include the observation of a diagenetic boundary within the Shikoku Basin sediments that may be compared to one documented further west by ODP Legs 131, 190 and 196 but occurs here at a lower temperature. Borehole heat flow measurements confirm spatial variations in the Shikoku Basin that were indicated by short probe surveys. Heat flow variations bet-ween topographic highs and lows may be related to fluid con-vection within the basement. This expedition also included the objectives of the Nankai Trough Submarine LandSLIDE history (NanTroSLIDE) Ancillary Project Letter (APL) and cored at Site C0018 a pile of mass transport deposits on the footwall of the megasplay fault, a major out of sequence thrust that presumably slips coseis-mically during large subduction earthquakes. This brought new insight on the timing of these mass wasting events and on the deforma-tion within the sliding slope sedi-ments.

Introduction and Goals

To improve our understanding of earthquakes and tsunamis generated by subduction mega-thrusts, an ambitious project known as NanTroSEIZE was initiated along the subduction boundary of southwestern Japan in the Kumano transect area (Fig. 1). The overarching goal of NanTroSEIZE is to create a distrib-uted observatory spanning the updip limit of seismogenic and tsunamigenic behavior (Tobin and Kinoshita, 2006a, 2006b). This multi-stage project is in the process of documenting several key com-ponents of the subduction margin, including the pre-subduction inputs of sediment and oceanic basement (Underwood et al., 2010), and the plate interface at shallow depths and at depths of 6–7 km where earth-quakes occur (Tobin et al., 2009).
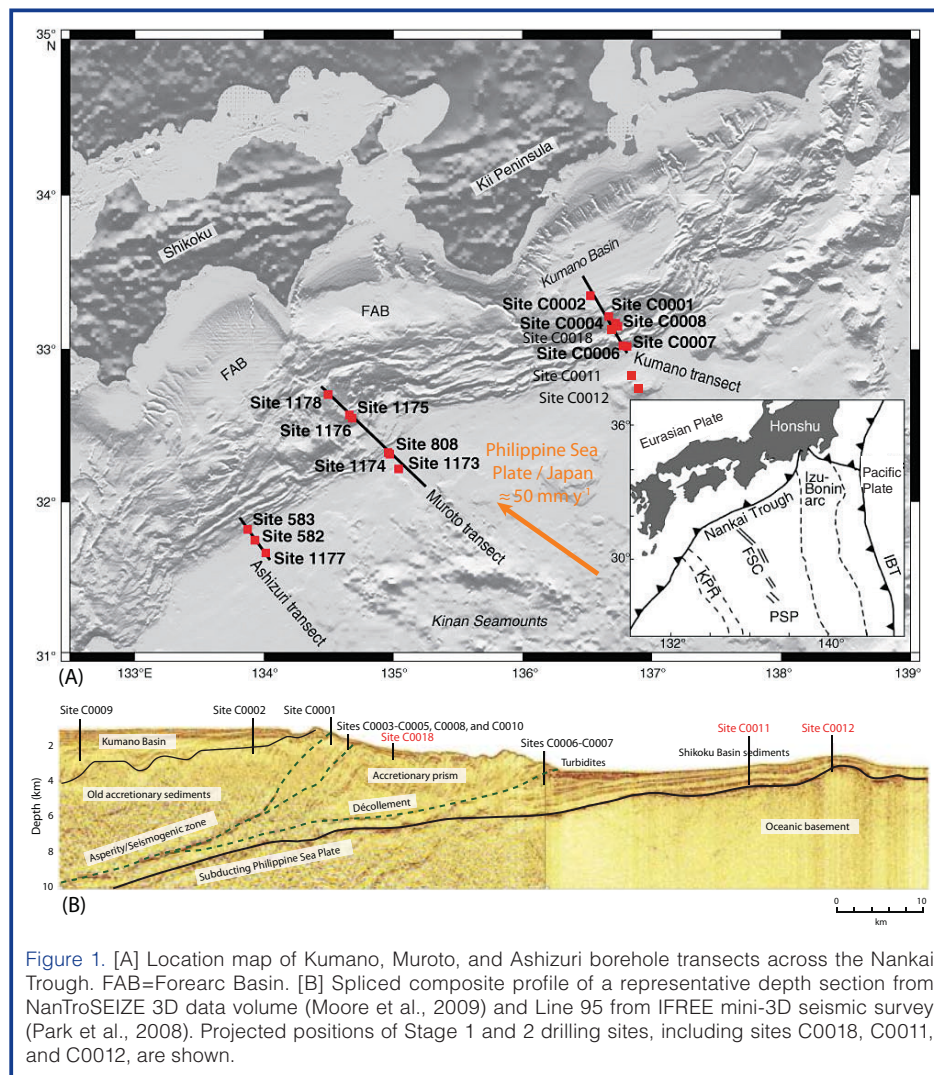

Figure 1. [A] Location map of Kumano, Muroto, and Ashizuri borehole transects across the Nankai Trough. FAB=Forearc Basin. [B] Spliced composite profile of a representative depth section from NanTroSEIZE 3D data volume (Moore et al., 2009) and Line 95 from IFREE mini-3D seismic survey (Park et al., 2008). Projected positions of Stage 1 and 2 drilling sites, including sites C0018, C0011, and C0012, are shown.

Exp. 333 addressed objectives at the NanTroSEIZE input sites seaward of the trench, Sites C0011 and C0012, as well as examined slope instability processes and their relationship with tectonic evolution proposed in the NanTroSLIDE APL. The characterization of the sedimentary column and ocean crust entering the subduction is essential because their evolution at increasing temperature and pressure presumably controls the transition to seismogenic behavior (Hyndman et al., 1997). Furthermore, the distribution of slip during earthquakes on faults affecting the shallow portion of subduction complexes determines locations of tsunami generation and their amplitude (Baba et al., 2006). The depth and frictional properties of the plate boundary fault and of splay faults connected to it may be controlled by the composition of incoming sediments, their diagenetic history, and the release and migration of fluids (Underwood, 2007). Heat flow is a vital measurement for the interpretation of diagenetic history, and it can also aid in identifying vigorous fluid circulation. Heat flow within the oceanic plate is also an important parameter for models calculating temperature along the subduction plate to the depth of the seismogenic zone (Hamamoto et al., 2011; Harris et al., 2011). This was not accurately constrained prior to this expedition.

The NanTroSLIDE APL arose from evidence gathered during earlier NanTroSEIZE drilling. IODP Expedition 316 found slumping near the fault scarp of the mega-splay, and 3D seismic reflection data revealed related mass transport deposits located further downslope (Strasser et al., 2011). Interpretation of 3D reflection seismic data and drilling results document a complex temporal and spatial evolution of the shallow mega-splay fault zone (MSFZ) and anticline structures in the underlying accretionary prism. This is characterized by a general decrease of thrusting motion with time since 2 Ma and alternating periods of high and low structural activity on individual structural segments (Strasser et al., 2009; Kimura et al., 2011). Site C0018 was drilled and cored to recover a Pleistocene-to-Holocene succession of stacked mass-transport deposits (MTDs) within a slope basin on the footwall of the megasplay thrust. Overall, drilling at Site C0018 aimed at (i) establishing a well-dated Quaternary submarine landslide history as it may relate to the tectonic evolution of the accretionary prism and (ii) reconstructing sliding and transport dynamics of submarine landslides as they may relate to the tsunamigenic potential of such event (Henry et al., 2010).

The specific set of questions addressed by Exp. 333 drilling is as follows.

- Is fluid circulation in basement and permeable sedimentary layers influencing heat flow and diagenesis at Sites C0011 and C0012?

- How does lithologic variation and diagenesis impact the physical properties of incoming sediments and guide fault development?

- Was magmatic activity heterogeneous in composition and age on the backarc basin basement high (Kashinosaki Knoll)?

- Is alteration of the upper oceanic basement heterogeneous, and how does such alteration influence geochemical and fluid budgets?

- What is the frequency of submarine landslides, what controls type, size, and magnitude of turbites and MTDs, and how do related processes change through time?

- How do large MTDs relate to the timing of splay fault activity as inferred from NanTroSEIZE Stage 1 drilling?

- What are the dynamics of large submarine landslides, and can we infer their tsunamigenic potential?

Geologic Setting and Previous Work

The Nankai Trough is a convergent plate boundary where the Philippine Sea Plate underthrusts the southwestern Japan margin. At the Kumano transect across the Nankai Trough, the velocity between the Philippine Sea Plate and the forearc is 4.5–5.5 cm y^{-1} along an azimuth of $305° \pm 3°$ (Seno et al., 1993; Mazzotti et al., 2001; DeMets et al., 2010; Loveless and Meade, 2010) down an interface dipping $3°–7°$ (Kodaira et al., 2000b). The subducting lithosphere of the Shikoku Basin was formed by backarc spreading during a time period of 15–25 Ma (Chamot-Rooke et al., 1987; Okino et al., 1994). The three major seismic stratigraphic sequences identified in the northern Shikoku Basin are the lower and upper Shikoku Basin facies and local spill-over of Quaternary trench-wedge turbidites (Ike et al., 2008a). The lower part of the Shikoku Basin displays a complex geometry influenced by basement topography (Ike et al., 2008b). Basement highs are also imaged within the subduction zone (Kodaira et al., 2003; Dessa et al., 2004), where they influence margin structure (Lallemand et al., 1992; Le Pichon et al., 1996; Park et al., 1999; Mazzotti et al., 2002; Bangs et al., 2006; Moore et al., 2009) and seismicity (Kodaira et al., 2000a; Park et al., 2004). The NanTroSEIZE expeditions focused on the Kumano transect, while earlier Ocean Drilling Program (ODP) and Deep Sea Drilling Project (DSDP) sites were drilled on the Muroto transect and the Ashizuri transects, respectively, in the central and western part of Shikoku Basin (Fig. 1; Moore et al., 2001). The combined data provide some information on input sediment variability at basin scale that may relate with margin structure. On the Kumano transect, swath bathymetry and multichannel seismic (MCS) data show a pronounced and continuous outer arc high extending >120 km along strike and marking the limit between the lower forearc slope and the forearc basin. The outer arc-high coincides with a splaying system of thrust faults that branch from a strong seismic reflector interpreted as a major out of sequence thrust, the megasplay fault (Park et al., 2002; Moore et al., 2007). Constraints on the slip

history of faults are a major outcome of the previous NanTroSEIZE expeditions. The lower forearc slope of the Nankai Trough consists of thrust imbricates that were accreted to the margin over the last 2 Ma (Kinothis et al., 2009; Moore et al., 2009) but since 400,000–700,000 a, this wedge has been thrust over the trench sediments without accretion of new imbricates (Screaton et al., 2009). NanTroSEIZE expeditions also showed slip on the megasplay is roughly synchronous with outer arc high uplift and subsequent Kumano forearc basin filling and tilting (Strasser et al., 2009; Gulick et al., 2010); however, in detail, long-term slip rates on individual splay thrust branches vary both in time and space (Kimura et al., 2011). The splay fault branch that was drilled slipped at rates ranging from 9 m kyr^{-1} to 2 m kyr^{-1} in the 2–1.5 Ma interval, but only at a very low rate (<100 m Ma^{-1}) over the last 1.3 Ma.

Exp. 322 and 333 focused on two sites on the subducting Philippine Sea Plate. Site C0011 is located on the northwest flank of a prominent bathy-metric high (the Kashinosaki Knoll; Ike et al., 2008a), whereas Site C0012 is located near the crest of the knoll (Fig. 2). Portions of Sites C0011 and C0012 were drilled and cored during Exp. 322 in 2009, but important intervals were not recovered, and heat flow data were not obtained. The upper part of the sedimentary sections was either washed down or cored with rotary core barrel (RCB), which yielded cores of insufficient quality in the shallow unconsolidated sediments. The basement was reached at Site C0012 on top of the Kashinosaki Knoll and cored at 538–576 m below seafloor (mbsf). As a result, IODP Exp. 333 aimed to fill gaps in core data on the upper part of the sedimentary section, acquire much-needed measurements of borehole temperature to assess thermal history and the extent of *in situ* diagenesis, and drill and core to a deeper level in basement at Site C0012 to assess heterogeneity in composition and alteration.

Although the stratigraphic coverage was incomplete, the merger of lithofacies and age-depth models shows how correlative units change from an expanded section at Site C0011 to a condensed section at Site C0012 (Fig. 3). The composite section also captured a previously unrecognized interval of late Miocene volcaniclastic sandstone. An older (early–middle Miocene) turbidite sandstone/siltstone facies with mixed volcaniclastic-siliciclastic detrital provenance occurs in the lower Shikoku Basin facies; this unit may be broadly correlative with superficially similar Miocene turbidites on the western side of the basin (Fergusson, 2003; Underwood, 2007; Underwood et al., 2010). The age of basal
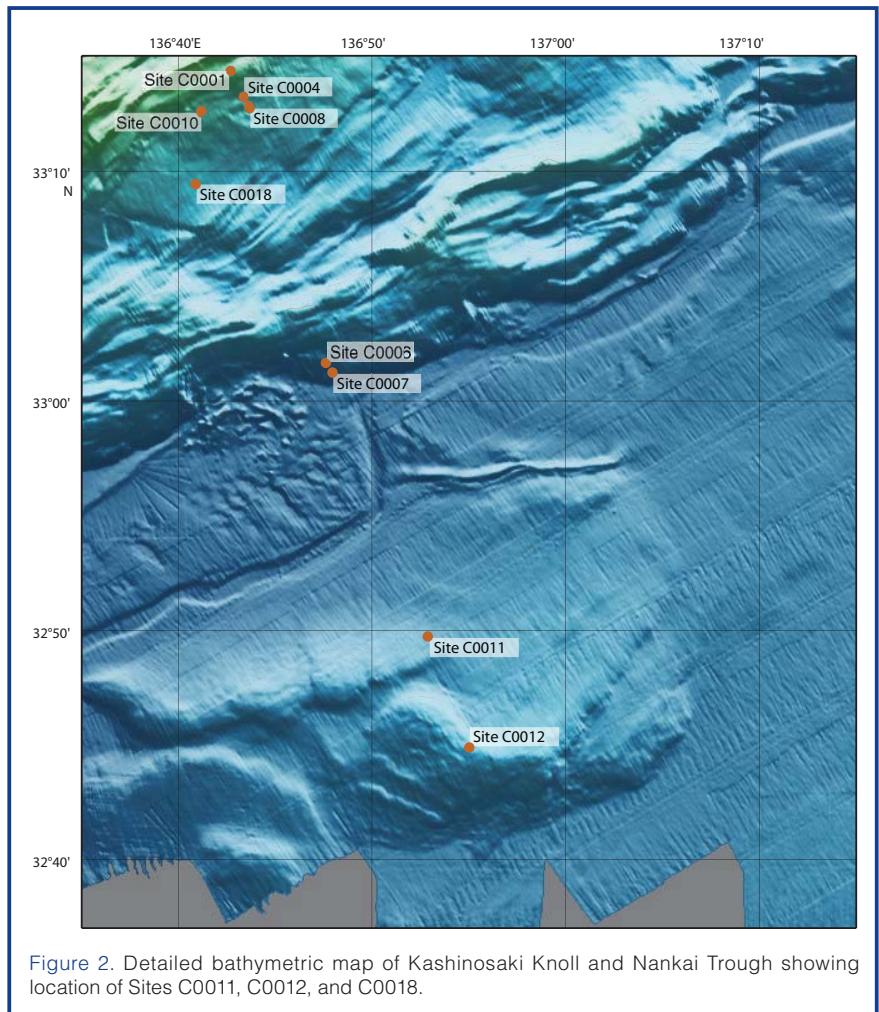

Figure 2. Detailed bathymetric map of Kashinosaki Knoll and Nankai Trough showing location of Sites C0011, C0012, and C0018.

sediment (reddish-brown pelagic claystone) at Site C0012 is older than 18.9 Ma.

Geochemical analyses of interstitial water on top of the basement high show clear evidence of upward diffusion of sulfate and other dissolved chemical species from the basement (Underwood et al., 2010). The depth of the sulfate reduction zone is also anomalously deep at Site C0012. Chlorinity values increase toward basement because of hydration reactions in the sediment and diffusional exchange with basement fluids (Underwood et al., 2010). In contrast to Site C0011, where chlorinity decreases with depth, the more saline fluids at Site C0012 are largely unchanged by the effects of focused flow and/or *in situ* dehydration reactions associated with rapid burial beneath the trench wedge and frontal accretionary prism.

Site C0018 is located ~3 km seaward from the splay-fault tip in a slope-basin that (1) represents the depocenter for downslope mass transport from the MSFZ, (2) is characterized by several MTDs identified in 3D seismic data (Strasser et al. 2011), and (3) includes an exceptionally large (as thick as 180 m) MTD. Drilling at Site C0018, which is located where the MTD bodies wedge out and where basal erosion is minimal, allowed for ground truthing and dating of the seismic-stratigraphic interpretation and sampling the MTDs

across the most complete and thickest stratigraphic succession.

Site C0011

A total of 380 meters of sediment was drilled in Holes C0011C and C0011D (Fig. 4). Two lithologic units were identified with very good recovery rates (Expedition 333 Scientists, 2012a). Unit I corresponds to Shikoku Basin hemipelagic/pyroclastic facies, and Unit II corresponds to a volcanic turbidite facies that was originally designated middle Shikoku Basin facies (Underwood et al., 2010). In addition, two lithologic subunits were interpreted within Unit I, Subunit IA (younger) and Subunit IB. Cored lithologies include silty clay, clayey silt, clay, and mudstone interbedded with coarse to fine volcanic ash. The Subunit IA/IB boundary occurs at 251.52 mbsf and separates more indurated dark gray mud and mudstone from overlying sediments that are highly bioturbated. The sediments below the transition are also marked by the disappearance of volcanic ash layers with unaltered glass. Below 347.82 mbsf, which is the Unit I/II boundary, there is an abrupt shift into coarser-grained tuffaceous sandstone and heterolithic gravel and sand.

Four volcanic ash layers comprise provisional stratigraphic markers at Site C0011; they were correlated with dated ash layers on land (Fig. 4). These are Azuki (0.85 Ma), Pink (1.05 Ma), Habutaki (2.8–2.9 Ma) and Ohta (4.0 Ma) (Hayashida, 1996; Satoguchi et al., 2005; Nagahashi and Satoguchi, 2007). Shipboard paleomagnetic interpretations and nannofossil biostratigraphy, done post-cruise, agree well with these preliminary identifications. The shipboard paleomagnetic interpretation also has good continuity with Exp. 322 data and yields an age of 7.6 Ma for the transition

between lithologic Units I and II, and the age of the Subunit IA/IB boundary is constrained to 5.32 Ma.

Structural features encountered in Hole C0011C and C0011D are rather sparse. Two sets of conjugate normal faults, striking NNE to SSW and NW to SE can be distinguished. The strikes of these conjugate sets are, respectively, parallel to the N25° maximum horizontal stress direction inferred from borehole breakouts at Site C0011 (Saito et al., 2010), and parallel to Nankai subduction convergence (300°–310°N; Mazzotti et al., 2001; Loveless and Meade, 2010). A NNE to SSW compression would be consistent with the local direction of compression inferred from kinematic modeling of the Zenisu-Izu fault system (20°N; Mazzotti et al., 2001). Furthermore, focal mechanisms of the 2004 earthquakes off the Kii Peninsula, which occurred within the oceanic plate north and northeast of Site C0011, indicate dominantly north–south compression (Ito et al., 2005). It is therefore likely that the state of stress at Site C0011 is influenced by intraplate compressive deformation within the Philippine Sea Plate.

Bulk density and resistivity values generally increase from the surface to 50 mbsf, reflecting normal consolidation of sediment. However, from ~50 mbsf to 80 mbsf density and resistivity decrease and then remain constant from 80 mbsf to 240 mbsf. Below 240 mbsf, density and resistivity increase abruptly across the transition between Subunits IA and IB and then continue along a normal consolidation trend. Two transitions were shown by logging-while-drilling (LWD) data at Site C0011 (Saito et al., 2010): one at 212 mbsf (downward decrease in gamma ray with a small associated decrease in resistivity) and one at 251.5 mbsf (downward increase in resistivity and gamma ray). The transition at 251.5 mbsf correlates with the abrupt porosity and resistivity change observed across the lithologic transition. However, the upper transition is not correlated with any remarkable observations on cores. During hydraulic piston coring system (HPCS) operations, downhole temperature was measured with the third-generation advanced piston corer temperature (APCT-3) tool at ~30-m intervals. We completed one measurement in Hole C0011C at 22.5 mbsf and eight measurements in Hole C0011D from 49 mbsf to 184 mbsf. Data show a nearly linear increase in temperature with depth (0.0913°C m^{-1}; Fig. 5), corre-
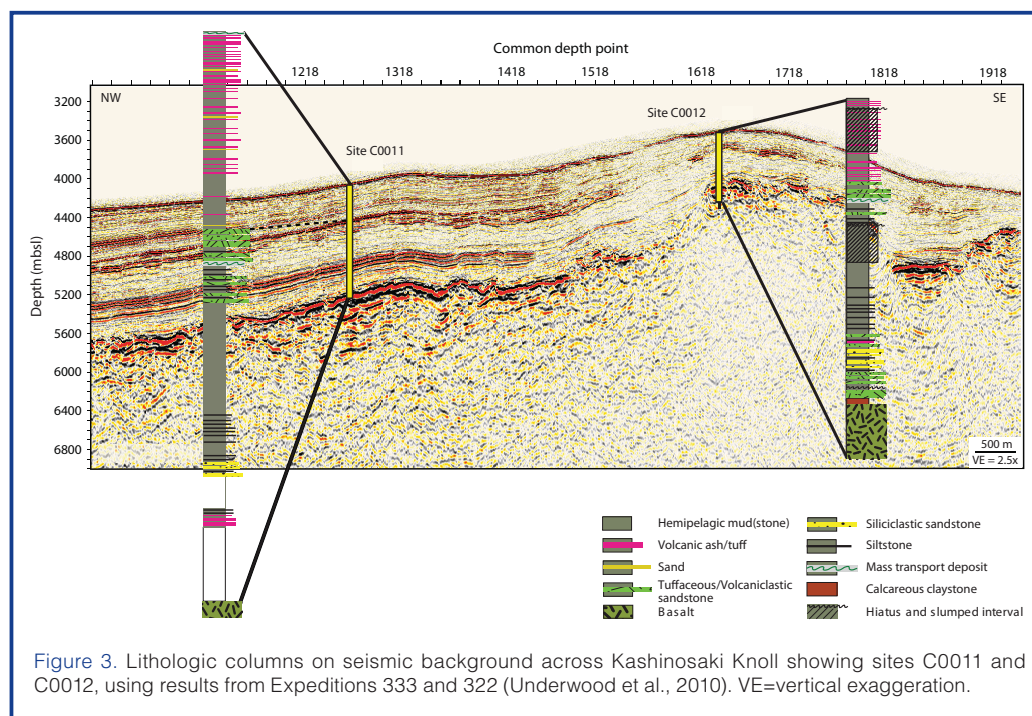

Figure 3. Lithologic columns on seismic background across Kashinosaki Knoll showing sites C0011 and C0012, using results from Expeditions 333 and 322 (Underwood et al., 2010). VE=vertical exaggeration.

sponding to a heat flow value of 89.5 mW m^{-2}. Temperature extrapolated at basement (~1050 m, from seismic profile), taking into account heat conductivity variations in the cored intervals, is ~80°C.

Interstitial water chemical composition trends are generally consistent with Exp. 322 results (Underwood et al., 2010). Chlorinity increases rapidly with depth in the upper ~25 m of Holes C0011C and C0011D, stays close to seawater value from 25 mbsf to 250 mbsf, and then gradually decreases. The chlorinity decrease, which continues to the deeper interstitial waters of Hole C0011B taken during Exp. 322 (Underwood et al., 2010), may reflect the updip migration of interstitial water freshened by the smectite-illite reaction at greater depths below the trench and prism toe. Sulfate concentration decreases rapidly in the upper 70 m of Hole C0011C, followed by a less dramatic decrease from 70 mbsf to 183 mbsf, which corresponds to the end of HPCS coring. The scatter of sulfate concentration below this level reflects seawater intrusion resulting from disturbance during coring. Yet sulfate probably remains present at low concentrations down to 280–300 m depth, which could explain why barium concentrations remain low and rise sharply below this level. Methane was the only hydrocarbon gas detected in holes C0011C and C0011D. It occurs only in low concentrations (2 ppmv) in the uppermost 260 m of the cored sequence and then rises to reach the highest values (~900 ppm) at the bottom of Hole C0011D. This indicates that, although sulfate consumption rate may be maximal at 70–80 m, the sulfate-methane transition zone occurs deeper, in the 250–300 m depth range.

Another remarkable feature is a sharp drop in silica concentration from ~800 ppm to ~200 ppm or less at the level of the transition from lithologic Subunit IA to IB. This drop correlates with a decrease in porosity from ~65 % to ~55 % observed over <10 m in moisture and density data, and with a concurrent resistivity increase in LWD (Saito et al., 2010) and core data. This behavior is similar to that observed at ODP Leg 190 Sites 1173 and 1177, where the base of the zone showing retarded compaction was ascribed to dissolution of opal-CT cement and precipitation of quartz (Spinelli et al., 2007). At the level of the tuffaceous sand-stones (350–370 mbsf), a second-ary silica concentration maximum is observed, which may be related to ash alteration.

Site C0012

In Holes C0012C and C0012D, 180 meters of lithologic Unit I (hemipelagic/pyroclastic facies) and the upper part of lithologic Unit II (volcanic turbidite facies) were drilled during Exp. 333 (Figs. 3, 4; Expedition 333 Scientists, 2012b). The remaining
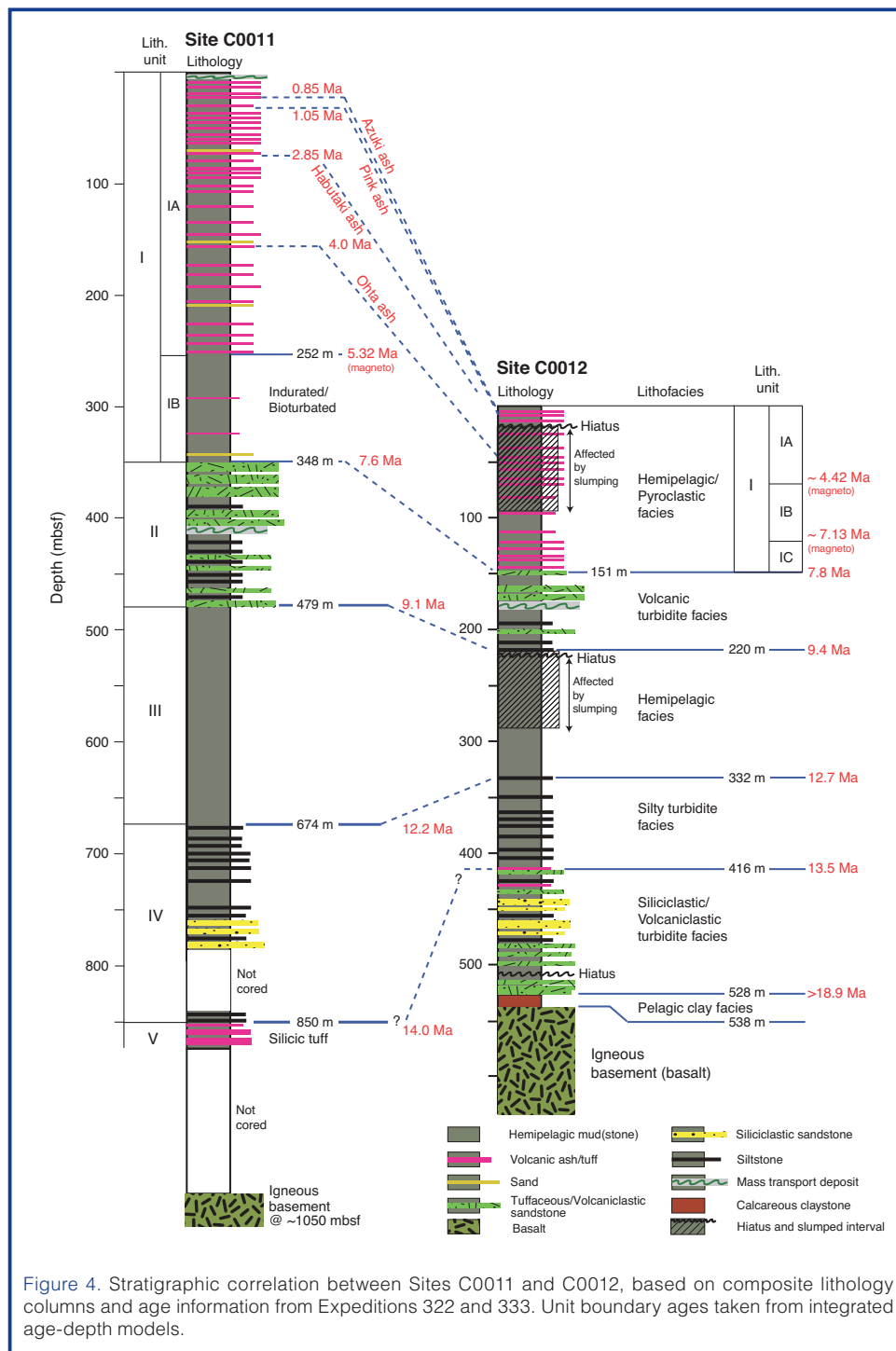

Figure 4. Stratigraphic correlation between Sites C0011 and C0012, based on composite lithology columns and age information from Expeditions 322 and 333. Unit boundary ages taken from integrated age-depth models.
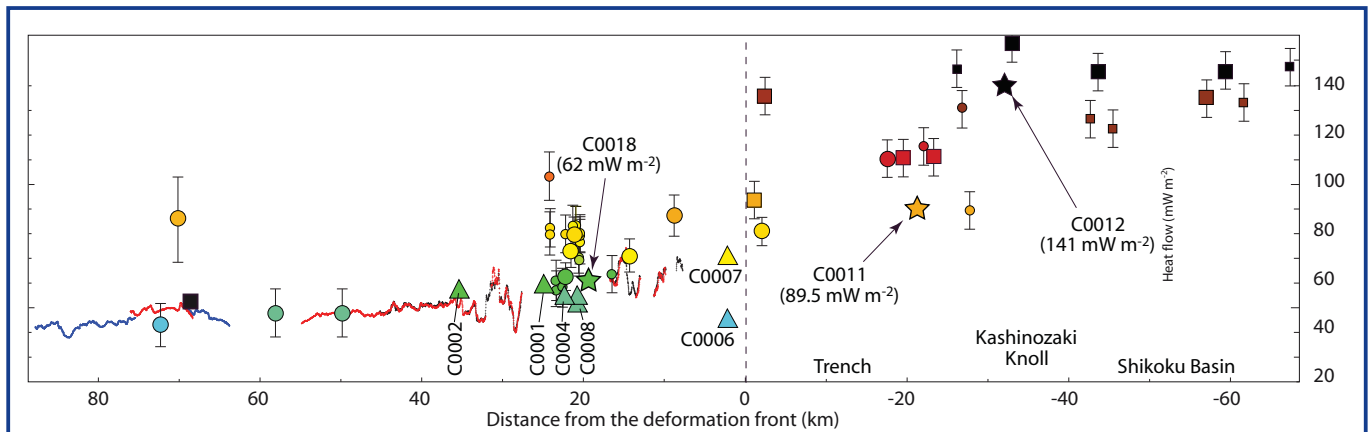
Figure 5. Heat-flow data collection in a 10-km-wide swath along the Kumano transect. Squares are heat flow probe measurements from Kinoshita et al. (2008), circles are long-term measurements from Hamamoto et al. (2011), triangles are borehole measurements from IODP Exp. 315 and 316, stars are from Exp. 333. The symbol sizes indicate data quality as defined by authors (big: good to excellent; small: poor to fair), the symbol color is a function of the heat flow value. Values derived from Bottom Simulator Reflectors (BSRs) along sections of multichannel seismic lines are plotted as lines.

holes (C0012E, C0012F, and C0012G) aimed at drilling red calcareous claystone and basalt at the contact between sediments in the Shikoku Basin and the igneous oceanic crust. Three lithologic subunits were interpreted in Unit I: Subunit IA (youngest), Subunit IB, and Subunit IC. The subunits are distinguished based on the presence, frequency of occurrence, and thickness of volcanic ash layers. The lithologies in Holes C0012C and C0012D include dark greenish gray clay and silty clay and silt interbedded with volcanic ash and minor occurrences of thin sand beds. A major decrease in the frequency of the occurrence of ash layers is recorded at ~71.5 mbsf, thereby defining the Subunit IA/IB boundary. Ash alteration was observed from 91.2 mbsf to the lower part of Subunit IB. At Site C0011, a comparable alteration front occurs at the top of Subunit IB. Ash layers are scarce to ~123.3 mbsf, which defines the base of Subunit IB. Another interval of dark greenish gray clay/silty clay-bearing ash layers corresponding to Subunit IC extends to 149.77 mbsf. This depth for the base of Unit I matches closely with the designation of 150.9 mbsf that was made during Exp. 322 (Underwood et al., 2010). Below 149.77 mbsf, Unit II comprises turbidite sands and sandstones with sharp and well-defined upper and lower boundaries. Commonly, beds have normal grading, but some comprise massive intervals with or without clay clasts. At the base of normally graded beds, pebble and sand clasts are composed of coarse ash and lapilli tuff. The lower part of Unit II comprises several layers of carbonate-cemented sandstones with calcite and barite veins. These beds are separated by mudstone very similar to that of Subunit IC.

Hole C0012E recovered two cores of greenish yellow mudstone intercalated with thin sandstone layers from 500 mbsf, corresponding to the base of lithologic Unit V (volcaniclastic-rich facies) defined during Exp. 322 (Underwood et al., 2010), and one core from 519 mbsf that recovered 6.8 m of reddish brown calcareous claystone with lighter green layers, overlying altered pillow basalts. The interface between the red calcareous claystone and the

basaltic basement was also recovered in Holes C0012F and C0012G. The red calcareous claystone corresponds to Exp. 322 lithologic Unit VI (pelagic claystone; Underwood et al., 2010) and contains veins of calcite with traces of barite as well as several layers with accumulations of manganese oxide forming millimeter- to centimeter-sized lumps.

Hole C0012G cored pillows and massive phyric basalts from 525.69 mbsf to the base of the hole at 630.5 mbsf. Two units are defined in the basalt: Unit I is composed of phyric or highly phyric pillow basalt, and Unit II is composed of sheet flows with pillow basalt interlayers. As observed during Exp. 322, the basalt in Unit I is highly altered, and some voids remaining between basalt pillows are filled with analcime. Observations of thin sections showed that all olivine and most glass as well as a fraction of the plagioclases have been replaced by secondary phases—dominantly saponite, celadonite and zeolites—that are also present as vesicle fillings. In Unit II, the massive sheet flows are more crystalline and generally less altered. Basalt experienced localized alteration under iron oxidizing conditions with accumulation of iron hydroxides in veins and alteration halos. Celadonite and saponite are present in the rock mass and, locally, pyrite. This suggests two stages of alteration, under iron oxidizing and iron reducing conditions.

Bedding planes at Site C0012 display a large range of dipping angles from 3° to 70° but are organized in zones of low and high bedding dips. Bedding planes with low dips are characteristically observed between 0 mbsf and 14 mbsf and between 85 mbsf and 145 mbsf. High-dip angle beds are found between 14 mbsf and 85 mbsf where they consistently strike northeast–southwest and dip southeast, and between 145 mbsf and 180 mbsf, where the distribution of strikes and dips appears scattered. Chaotic structures (disrupted beds, folds, and injections of sand or mud) are observed at the bottom of the high-dip angle sections. Faults and shear zones mostly display normal displacement with high-dip angles, striking northwest–southeast, and dipping northeast or
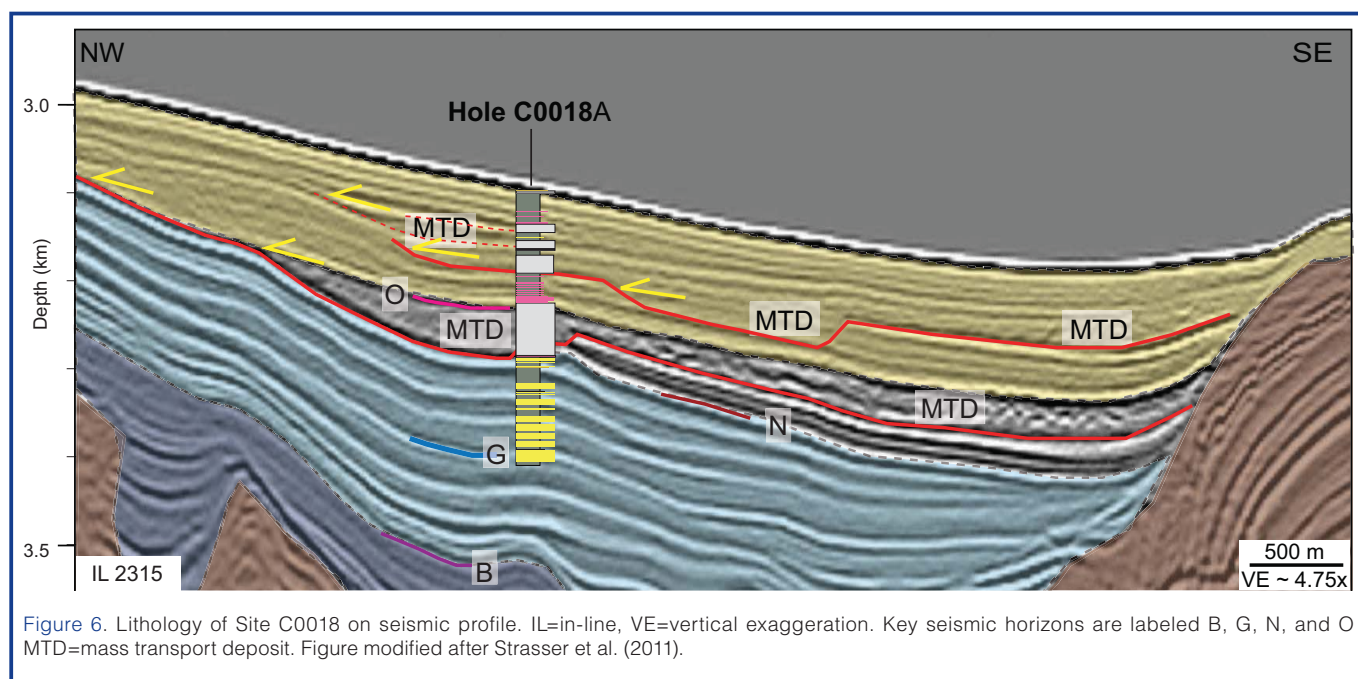
southwest, suggesting northeast–southwest extension. Considering the location of Site C0012 on a topographic high southwest of a steep arcuate slope evocative of a slide scar (Fig. 2), the interpretation proposed is that the high-dip angle sections have been affected by sliding events.

The cored portion of Units I and II has an estimated Holocene–Late Miocene age range (~0–8.3 Ma). Three ash beds were correlated to known tephra dated on land, based on visual observations of the shape of the glass shards and dominant associated minerals in smear slides. The Azuki volcanic ash bed, dated on land as 0.85 Ma (Hayashida et al., 1996), was identified at 5.7 mbsf. The Pink ash bed, dated on land as 1.05 Ma (Hayashida et al., 1996), correlates with a characteristic ash bed at 7.7 mbsf. A third major volcaniclastic event, the Ohta ash bed, dated on land as 4.0 Ma (Satoguchi et al., 2005), correlates with an ash bed at 44.95 mbsf. The unusually shallow depths of the presumed Azuki and Pink ash beds imply very slow average sedimentation rates over the last ~1 Ma. This interpretation is, however, consistent with the depth of the Brunhes-Matuyama reversal and of the Jaramillo Chron from natural magnetic remanence data. This interval of condensed sedimentation lies on an angular unconformity at ~14 mbsf, interpreted as the top of a slump. Paleomagnetic and biostratigraphic data suggest that this unconformity correlates with an age hiatus of ~2.0 m.y. (~1 Ma to ~3 Ma). Similar observations within the upper part of Unit III during Exp. 322 suggested that a slumping event associated with the remobilization of the uppermost sedimentary layers also occurred about 9.5 m.y. ago (Underwood et al., 2010). The transition from Subunit IA to IB is constrained at 4.42 Ma from magnetostratigraphy, and thus appears slightly younger at Site C0012 than at Site C0011. The change of the frequency of ash layer occurrence at the Subunit IB/IC boundary is constrained to 7.13 Ma from magnetostratigraphy. The age models at the depth of the transition from Unit I to Unit II are very consistent, and they provide an age of 7.8 Ma, slightly older than at Site C0011.

Porosity and resistivity measured on cores at Site C0012 present, as at Site C0011, an anomalous interval where these parameters remain constant with depth and do not follow a progressive compaction trend, whereas shear strength increases. This interval is found at a shallower depth range (~10 mbsf to 70 mbsf), and it displays a more progressive transition at its base from ~70 mbsf to 100 mbsf across the lithologic Subunit IA/IB boundary. Site C0012 porosity values from below 240 mbsf are generally lower than those from similar depths at Site C0011. A possible explanation for this observation is the removal of about 100 meters of overlying material by erosion or slope failure. This interpretation would be consistent with the observed time gap of ~2 m.y. found between 10 mbsf and 14 mbsf. Near the base of the sediments, calcareous claystones cored below 500 mbsf range in porosity from 0.28 to 0.46 and show P-wave velocities of ~2000 m s^{-1}. Within the basalt, measured porosity is extremely variable and ranging from 0.09 to 0.37, and measured P-wave velocities vary between 3000 m s^{-1} and 5000 m s^{-1}.

Thermal gradient values are evaluated from the APCT-3 measurements made at ten depths in Holes C0012C and C0012D together, and the mean thermal gradient value determined is 0.135 K m^{-1} (Fig. 5). The estimated heat flow value at this site is 141 mW m^{-2}, amounting to ~50% higher than the 89.5 mW m^{-2} determined for the adjacent Hole C0011C that was drilled during this expedition. Based on the determined heat flow value of 141 mW m^{-2}, as well as the thermal conductivity values from core measurements (Saito et al., 2010), temperature at the top of basement (at 526 mbsf) is estimated to be ~65°C, which is significantly lower than the estimated value of 80°C at ~1050 mbsf at Site C0011.

Figure 6. Lithology of Site C0018 on seismic profile. IL=in-line, VE=vertical exaggeration. Key seismic horizons are labeled B, G, N, and O MTD=mass transport deposit. Figure modified after Strasser et al. (2011).

As at Site C0011, results of interstitial water analysis are generally consistent between Exp. 333 and 322. Overall, the combined data sets reflect *in situ* alteration of volcanic ash in the sediment and basalt alteration in the upper igneous crust as well as exchange by diffusion (Underwood et al., 2010). The sulfate profile for Site C0012 indicates that sulfate reduction occurs at a deeper level than at the other sites drilled during this expedition. A minimum in sulfate concentration at ~300 mbsf was observed during Exp. 322, and this was interpreted as being driven locally by anaerobic methane oxidation (Underwood et al., 2010). In Holes C0012E and C0012A, sulfate increases in concentration in the interval below ~450 mbsf, which may indicate diffusional exchange with fluid in basaltic basement that sustain a higher sulfate concentration. A trend of increasing chlorinity, Ca, and Sr concentrations and decreasing Na in the lower part of the boreholes is also interpreted as a consequence of diffusion between the lowermost sediment and basement fluids. At a shallower level, samples from Hole C0012C document a silica concentration drop below the Subunit IA/IB boundary at ~70 m, where a decrease in porosity and an increase in resistivity are also observed. Alteration of volcanic glass shards also becomes more pronounced. As at Site C0011, this suggests a relationship between interstitial water composition, the presence or dissolution of opal-CT cement, and ash diagenesis.

In Holes C0012C and C0012D, methane and ethane were either below detection or present at only low concentrations. No heavier hydrocarbon gases (e.g., C3 and C4) were found. The only two samples that contained both methane and ethane were found at depths of ~501 mbsf and ~520 mbsf in
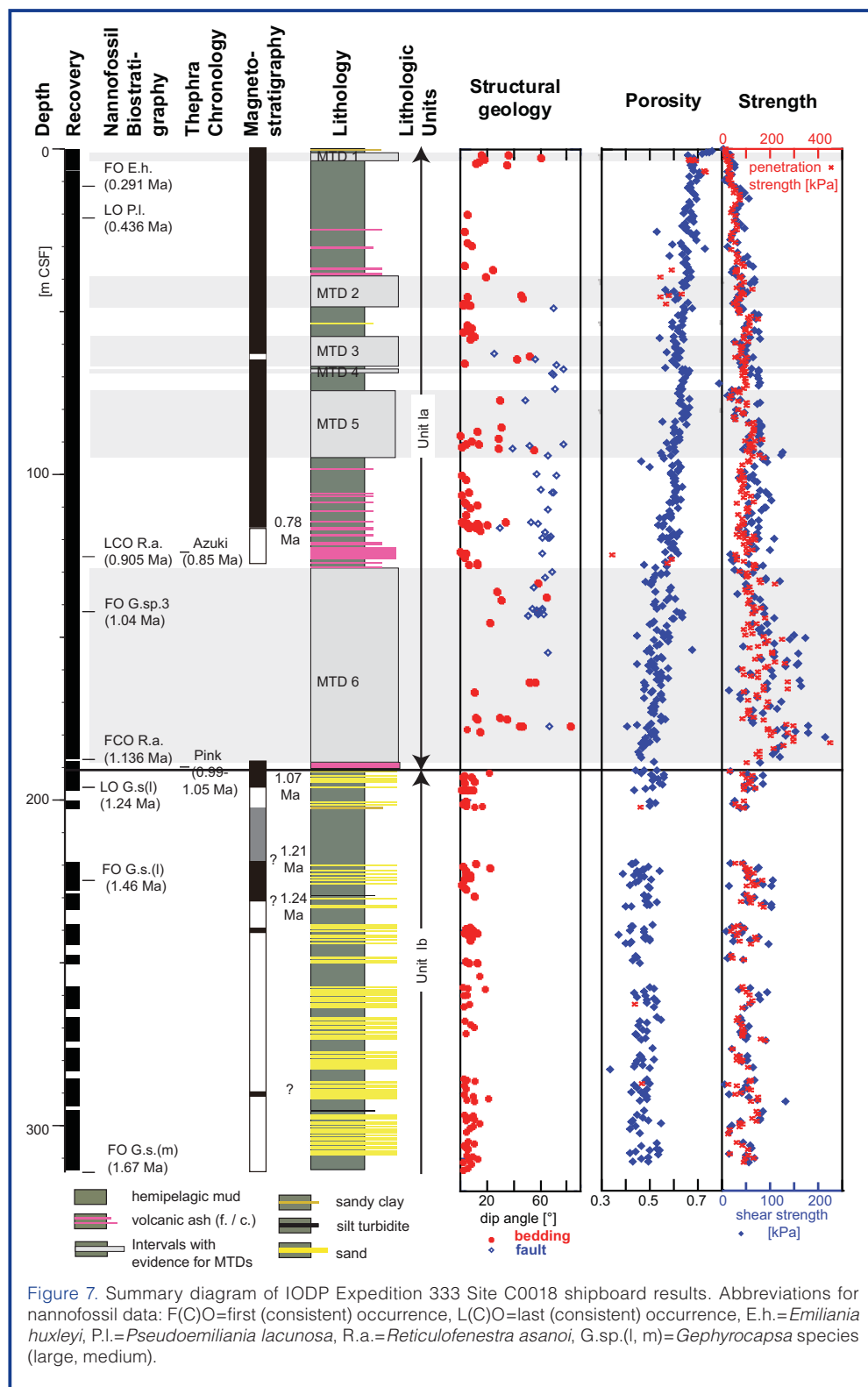

Figure 7. Summary diagram of IODP Expedition 333 Site C0018 shipboard results. Abbreviations for nannofossil data: F(C)O=first (consistent) occurrence, L(C)O=last (consistent) occurrence, E.h.=*Emiliania huxleyi*, P.l.=*Pseudoemiliania lacunosa*, R.a.=*Reticulofenestra asanoi*, G.sp.(l, m)=*Gephyrocapsa* species (large, medium).

Hole C0012E; they had C1/C2 ratios of <100, indicating a possible thermogenic origin of these hydrocarbon gases.

Site C0018

Sediments cored at Site C0018 (Fig. 6) are subdivided into two lithologic subunits (Expedition 333 Scientists, 2012c), which correlate with seismic Unit 1a and 1b of Kimura et al. (2011) and Strasser et al. (2011). Lithologic Subunit 1a is pri-

marily composed of bioturbated hemipelagic mud inter-calated with layers of varying coarse and fine volcanic ash. Six intervals with evidence of MTDs are observed within Subunit 1a (Fig. 7). MTDs at Site C0018 range in thickness from 0.5 m to 61 m and have a cumulative thickness of 98 m, thus accounting for half of the total thickness of Subunit 1a. MTD 6 correlates to the main MTD body identified in seismic data (Fig. 6; Strasser et al., 2011). The upper boundary/contact is well defined for MTDs 1, 2, and 6 and is marked by an MTD-overlying turbidite for two of them (MTDs 2 and 6). Shear zones in fine-grained sediments define the base of MTD 2, 3, and 5. Additionally, physical properties data (Fig. 7) show that MTD intervals display an increased compaction gradient (locally stronger porosity decrease with depth) compared with the linear porosity-depth trend which may be defined over the whole Subunit 1a, and slight reversals (porosity increasing with depth) are observed near the base of MTDs 2, 3, 5, and 6. A thick ash layer, which correlates to the onland tephra "Pink" dated 1.05 Ma (Hayashida et al., 1996), occurs at the base of MTD 6 and also defines the base of Subunit 1a at 190.6 mbsf. This age is supported by magnetostratigraphic constraints correlating the base of a short normal polarity interval immediately below the subunit boundary to the base of the Jaramillo subchron (1.07 Ma), and it is also consistent with the maximum age for this boundary estimated from calcareous nanno-fossils (<1.24 Ma). The Azuki ash layer (Hayashida et al., 1996) was identified above MTD 6, con-straining its emplacement between 0.85 Ma and 1.05 Ma. Unit 1a thus spans from 0 Ma to ~1 Ma, and the average sedi-mentation rate is ~19 cm ka^{-1}. Minor normal faults with moderate to high dip angles (50°–80°) are developed in the lower part of Subunit 1a; they reflect vertical maximum principal stress likely in response to the sedimentation and burial processes within the slope basin. Progressive burial and consolidation are indicated by the general downward increase and decrease of undrained shear strength and porosity, respectively (Fig. 7).

Lithologic Subunit 1b comprises a sequence of sandy turbidites interbedded with silty clay. Sub-horizontally dipping 4–20-cm-thick sand layers typically show a sharp and erosional base and normal grading. Bed spacing is 20–30 cm in average, but muddy intervals up to 4 m thick without intercalated turbidites occasionally occur. Turbidite sands have mixed composition with quartz, plagioclase, and abundant lithic fragments of both metamorphic and volcanic origin, indicating a siliciclastic source. Averaged sedimenta-tion rate within Unit 1b is ~40 cm ka^{-1}, higher than in Unit 1a. Porosity and undrained shear strength (measured in muddy intervals) are generally constant throughout Unit 1b, and they show values slightly higher and lower, respectively, than what would be expected from downward extrapolating the general trends from Unit 1a. The drop in shear strength below the subunit boundary may be related to the switch from HPCS at this depth to extended punch and extended shoe coring systems (EPCS, and ESCS, respectively), which

cause more disturbance to the cores. If real, however, this observation may be interpreted to reflect a general state of slight underconsolidation, potentially resulting from the high sedimentation rates within this interval and the deposi-tion of the thick MTD immediately above.

Key Results and Future Work

Shikoku Basin Stratigraphy and Diagenesis

Observations on HPCS, EPCS and ESCS cores comple-mented stratigraphic description in the upper part of the sedimentary columns drilled during Exp. 322. The new observations, however, did not bring major changes in the definition of lithologic units (Saito et al., 2010; Expedition 333 Scientists, 2011). The most remarkable new observa-tions is the correlation between a sharp variation of physical properties (porosity and electrical resistivity; Fig. 8), which was already evident in the LWD data from Exp. 319, a drop in silica concentration, and a concurrent decrease of the abun-dance of ash layers and increase of their state of alteration. Glass shards from ash layers generally appear fresh above, but are variably altered below, with evidence for glass disso-lution and replacement by clay minerals.
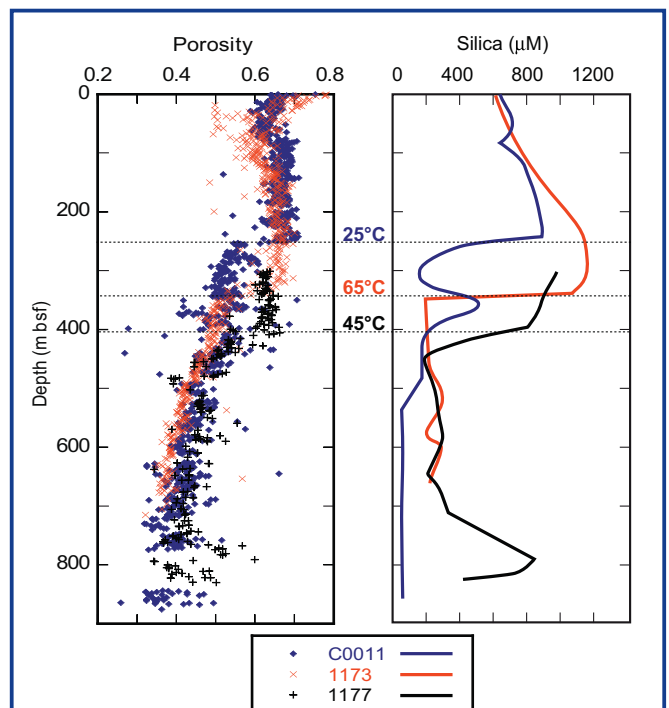

Figure 8. Porosity from sites C0011, 1173, and 1177 from moisture and density measurements, and silica concentration profiles in interstitial water. A concomitant drop of silica concentration and porosity is observed at all sites within the Shikoku Basin hemipelagites. This also correlates with a front of volcanic ash alteration. It was proposed that clay compaction is prevented by the precipitation of opal-CT cements at grain boundaries at the initial stages of diagenesis and that this metastable cement is then dissolved as temperature increases (Spinelli et al., 2007). The temperature estimated from borehole measurements at the depth of the transition is indicated. The diagenetic boundary is found at a different temperature at each site, which may help constraining the kinetics of the reactions.

The transition occurs within 10 m at 250 mbsf at Site C0011 but is found at a shallow level and is more progressive (50–80 m) at Site C0012. However, the sediment at this site has been affected by slumps, and this may preclude an accurate description of the transition. From an analogy with results obtained after Leg 190, it can be proposed that the process responsible for an anomalously high porosity of the sediment above this boundary is cementation by opal-CT and opal dissolution with precipitation of quartz below the boundary (Spinelli et al., 2007). However, the temperature of the reaction would be unusually low at Site C0011 (currently 25°C, as opposed to 65°C at Site 1173, see Fig. 8) and, assuming constant heat flow, it cannot be explained with the reaction kinetics used by Spinelli et al. (2007) because the kinetic time constants calculated at 25°C would be larger than the sediment age. The transition in physical properties is found at an even lower temperature (15°C) at Site C0012, but this may be in part explained by the removal of about 100 meters of sediment by the slump that occurred about 1 Ma ago. Furthermore, the primary silica source is dispersed volcanic glass rather than biogenic opal-A (White et al., 2011), and fresh glass is found again in volcaniclastic sands at a deeper level associated with high silica concentration in the interstitial water. It thus remains an open question whether the kinetics of the opal-A/opal-CT and opal-CT/quartz reactions can accurately model this transition. For instance, other kinetic models could be more appropriate for a volcanic ash silica source (Schacht et al., 2008). It is also possible that initial amorphous silica concentration immediately below the transition was too low to prevent compaction. Answering these questions will require postcruise work (e.g., amorphous silica content determination and modeling work). Chronostratigraphy based on paleomagnetism and biostratigraphy suggests that the age of the transition from opal-cemented hemipelagic mud with numerous ash layers to compacted hemipelagic mudstone with sparse ash layers at Site C0011 (5.25 Ma) is slightly younger at Site 1177 (4.5 Ma), the reference site for the Ashizuri transect. It is even younger at Site 1173 (2.5–3.0 Ma), the reference site for the Muroto transect, where higher heat flow and temperature can account for a more advanced silica diagenesis and result in an upward migration of the transition in the sedimentary column (Spinelli et al., 2007).

Overall, the temperature conditions at correlative stratigraphic levels do not vary by more than ~15°C between the two drill sites. Consequently, differences in fluid composition observed between the two sites (e.g., increasing versus decreasing chlorinity toward basement) cannot result solely from *in situ* reactions in the cored intervals. Temperature and heat flow determinations indicate that the temperature conditions in the uppermost basement at Site C0011 are within the temperature window for the onset of the smectite-illite reaction (~55°C–90°C), which has been proposed as the main cause of freshening at this site (Underwood et al., 2010). Although it is unlikely that the reaction has progressed to a significant extent in any of the cored sections,

illitization should thus be expected in the lower part of Site C0011, and it should continue into the trench where the Shikoku Basin sediments are buried to greater depths. Unfortunately, coring during Exp. 322 was aborted almost 200 m above the top of basement at Site C0011.

Heat Flow and Convection

Exp. 333 provided the first borehole temperature measurements on the incoming plate of the Kumano transect, which constitute an essential constraint for subduction thermal models. Estimation of heat flow was conducted from linear regression of temperature as a function of thermal resistance. Heat flow thus obtained shows a good correspondence with heat flow probe and instrumented corer data (Fig. 5; Kinoshita et al., 2008; Hamamoto et al., 2011). The 90 mW m^{-2} heat flow at Site C0011 is in the lower range of heat flow probe values, while the 140 mW m^{-2} heat flow at Site C0012 is one of the highest. This result confirms the presence of a high heat flow anomaly on the Kashinozaki Knoll. However, constraints on the age of the oldest sediments at the base of C0012 are compatible with Kashinozaki Knoll having the same age (about 20 Ma) as the lithosphere in this part of the Shikoku Basin as indicated from magnetic anomalies (Chamot-Rooke et al., 1987; Okino et al., 1994). When compared with models, heat flow at Site C0011 appears slightly lower that the heat flow expected for a 20-Ma lithosphere (Kinoshita et al., 2008) but can be fit within uncertainties once the effect of sedimentation in the trench is taken into account (Marcaillou et al., 2012). Large-scale heat transfer from depth within the subduction zone to the trench by convection in the crust, as proposed for the Muroto transect to the west (Spinelli and Wang, 2008), appears unlikely on the Kumano transect because the heat flow remains moderate in the trench. However, 1- to 10-km scale heat flow variability could be caused at least in part by thermal convection. Because pore fluid geochemistry profiles from Exp. 322 and 333 do not provide evidence for fluid transfer between Site C0011 and Site C0012 along sedimentary layers, local convection in the basement appears the most likely explanation for the presence of a heat flow maximum in the summit area of Kashinozaki Knoll.

The Sediment-Basalt Interface and the Basalt

The basalt-sediment interface was cored three times during Exp. 333 with ESCS in Hole C0012E, and with RCB in Holes C0012F and C0012G. Although coring with ESCS was not the original choice, it was used to make the best of a short workable window between two periods of bad weather, and it provided good recovery of altered basalt including the inter-pillow hyaloclastites and analcime filled cavities. Multiple sampling of the red clay above the basement allowed recovery of larger amounts of pore fluid, which will be used for shore-based characterization of fluid isotopic composition (strontium, lithium, dissolved inorganic carbon). From an operational point of view, the use of a polycrystalline

diamond compressed (PDC) bit turned out as inappropriate, as the bit was worn down to a point it was no longer functional even before basement coring started. As a consequence of weather-related and technical delays only two days were available for basement coring. One hundred meters were cored with patchy recovery. Pillows and massive flows of phyric basalt were recovered. As observed during Exp. 333, basalts were pervasively altered under iron reducing conditions, most of the glass, olivines, and part of the plagioclases being replaced by saponites and zeolites. Deeper penetration below the seafloor found occasional veins with accumulations of iron hydroxides. The sequence of alteration still needs to be determined. Knowledge of mineralogical composition of the altered basalt will allow quantifying fluid sources available from mineral reactions at the depth of the seismogenic zone, notably the saponite-chlorite reaction.

Mass Wasting and Mass Transport Deposits

The slope-basin stratigraphic succession drilled at Site C0018 documents ~1.5 million years of sedimentation by hemipelagic settling, turbidite, and mass-transport deposition in the footwall of the MGFZ. A lithological transition between a sandy turbidite sequence (below) and ash-bearing hemipelagites that contain MTDs (above) is dated to ~1 Ma (Fig. 7). Six MTDs of thickness 0.5–61 m were identified in the succession overlying this transition, but no positive evidence for MTDs within the turbidite sequence below has been found in the cores. During the same time period, a northward shift in the sediment depocenter is observed within the Kumano forearc basin following ~300 kyr of extensive landward tilting of the outer Kumano basin sediments. This has been interpreted to be related to an episode of motion along the megasplay that formed the modern fault geometry (Gulick et al., 2010). Hence, one possible explanation for the change in sediment delivery and routing pattern inferred from Site C0018 results is that the uplift of the outer arc high confined most of the turbidity currents to the Kumano Basin and thus progressively shut off sand input to the slope-basin seaward of the MSFZ (Strasser et al., 2012). Alternatively, the observed evolution could correspond to a local change of slope and depositional environment from a perched basin trapping sand transported by turbidity currents to a slope environment.

MTD 6 is correlative with this lithological transition and thus potentially may be related to the overall structural evolution of the MSFZ area and/or the change in sedimentation regime. However, all younger MTDs observed at Site C0018 postdate the main structural phase of slip on the shallow MGFZ and may be rather associated with shallow-seated slope failure processes within the post-1-Ma sedimentary cover overlying the MSFZ and anticline structure. The deformation style within these MTDs is heterogeneous; intervals of disturbed sediments are interbedded within intervals inferred to retain original, coherent bedding. In three occurrences the base of the MTD is defined by a shear zone

within fine-grained sediments. These observations suggest that slumping and mass-transport are dominated by localized plastic deformation and that slumping only partly evolved into mud flows.

Mass movements are actively shaping the present-day seafloor, as evidenced by numerous surficial slump scars (Kimura et al., 2011; Strasser et al., 2012) and the occurrence of a shallowly buried, presumably Holocene, MTD at Site C0018 (Strasser et al., 2012). Further important findings are that the spacing between individual MTDs suggests submarine slope destabilization does not occur systematically during subduction earthquakes that have a recurrence rate on the order of 100–200 years (Ando, 1975). Hence, yet-to-be-investigated preconditioning factors may exert first-order control on destabilization processes and MTD formation over the last 1 Ma and in the future. These preconditioning factors will be the focus of upcoming studies integrating higher-resolution age constraints, more detailed sedimentological and structural investigations of MTDs, 3D-seismic interpretation and seismic attribute analysis, geotechnical laboratory analysis, as well as data and results from nearby IODP drill sites.

Site C0012 also appears strongly influenced by mass wasting processes. Slumps affecting sediment packages of 70–80 m thickness were identified during Exp. 322 and 333. Their top is marked by hiatuses (from ~1 Ma to 3 Ma and around ~9.5 Ma, respectively), and an even longer hiatus is evident along an unconformity within Unit V near the base of the sedimentary section. Repetition of mass wasting events is very understandable considering the location of Site C0012 on a topographic high immediately above the edge of a major slide scar observed in the bathymetry and seismic data.

Summary and Conclusions

Borehole heat flow data from Exp. 333 constrain heat flow in the trench and provide a reliable seaward boundary condition for modeling of temperature along the subduction interface (Marcaillou et al., 2012). A sharp contrast in physical properties in the Shikoku Basin hemipelagites is interpreted as a diagenetic boundary, present throughout the basin, and related to the diagenesis of high-silica volcanic ash. This diagenetic boundary is diachronous, and the geometry of turbidite bodies in the lower part of the Shikoku Basin displays considerable variability (Underwood, 2007; Underwood et al., 2010). Nevertheless, an interval of sedimentation deprived of fresh volcanic ash and turbidites is found on the three transects investigated by IODP drilling in the Nankai area. This broadly corresponds to the 4–7 Ma time interval. This interval appears as a favorable interval for the localization of the decollement of the accretionary wedge but also for the localization of basal shear of slumps at Sites C0011 and C0012. Sampling of cores for geotechnical and mechanical tests will address this problem.

A sequence of cored mass transport deposits remobilizing slope sediments in the shallow MGFZ area documents ~1 million years of submarine landslides in this tectonically active setting (Strasser et al., 2012). Although earthquakes are an obvious potential triggering factor, these mass wasting events appear much less frequent than large earthquakes along this subduction segment. Thus, preconditioning factors such as sedimentation, tectonic loading, and fluid flow must exert key control on slope destabilization, and they are the focus of future investigations. Evidence from Sites C0011 and C0012 shows that large mass wasting events also occurred on topography on the downgoing plate and could explain some of the hiatuses observed within accreted sediment packages.

The basement appears altered by low temperature interaction with pore fluid of seawater origin over at least 100 m. Fluid convection is likely to occur in the fractured basement, but it constitutes a hydrological system largely distinct from the sediment, which comprises clay-dominated intervals that form barriers to flow, at least in the vertical direction. Release of water from mineral reactions will occur both in the sediment and in the basement, as they are buried below the sedimentations in the trench and underthrust beneath the margin. Modeling this evolution will likely be an important objective of post-cruise work.

The IODP Expedition 333 Scientific Party

Tiago Alves, Thorsten Bauersachs, Hugh Daigle, Koray Ekinci, Shu Gao, Marion Garcon, Kiichiro Kawamura, Yujin Kitamura, Jan Sverre Laberg, Gwangsoo Lee, Youngmin Lee, Yuehan Lu, Boris Marcaillou, Osamu Matsubayashi, Yoshitaka Nagahashi, Beth Novak, Yu Saito, Yasufumi Satoguchi, Elizabeth J. Screaton, Rachel P. Scudder, Bo Ra Song, Asuka Yamaguchi

Acknowledgements

References

Ando, M., 1975. Source mechanisms and tectonic significance of historical earthquakes along the nankai trough, Japan. *Tectonophysics*, 27:119–140. doi:10.1016/0040-1951(75)90102-X

Baba, T., Cummins, P.R., Hori, T., and Kaneda, Y., 2006. High precision slip distribution of the 1944 Tonankai earthquake inferred from tsunami waveforms: Possible slip on a splay fault. *Tectonophysic*s, 426(1–2):119–134. doi:10.1016/j.tecto.2006.02.015

Bangs, N.L.B., Gulick, S.P.S., and Shipley, T.H., 2006. Seamount subduction erosion in the Nankai Trough and its potential impact on the seismogenic zone. *Geology*, 34(8):701–704. doi:10.1130/G22451.1

Chamot-Rooke, N., Renard, V., and Pichon X.-L, 1987. Magnetic anomalies in the Shikoku Basin: A new interpretation. *Earth Planet. Sci. Lett.*, 83:214–228. doi:10.1016/0012-821X (87)90067-7

DeMets, C., Gordon, R.G., and Argus, D.F., 2010. Geologically current plate motions. *Geophys. J. Int.*, 181(1):1–80. doi:10.1111/j.1365-246X.2009.04491.x

Dessa, J.-X., Operto, S., Kodaira, S., Nakanishi, A., Pascal, G., Uhira, K., and Kaneda, Y., 2004. Deep seismic imaging of the eastern Nankai Trough, Japan, from multifold ocean bottom seismometer data by combined travel time tomography and prestack depth migration. *J. Geophys. Res.*, 109:B02111. doi:10.1029/2003JB002689

Expedition 333 Scientists, 2011. NanTroSEIZE Stage 2: Subduction inputs 2 and heat flow. *IODP Prel. Rept.*, 333. doi:10.2204/iodp.pr.333.2011

Expedition 333 Scientists, 2012a. Site C0011. *In* Henry, P., Kanamatsu, T., Moe, K., and the Expedition 333 Scientists, *Proc. IODP*, 333: Washington, DC (Integrated Ocean Drilling Program Management International, Inc.). doi:10.2204/iodp.proc.333.104.2012

Expedition 333 Scientists, 2012b. Site C0012. *In* Henry, P., Kanamatsu, T., Moe, K., and the Expedition 333 Scientists, *Proc. IODP*, 333: Washington, DC (Integrated Ocean Drilling Program Management International, Inc.). doi:10.2204/iodp.proc.333.105.2012

Expedition 333 Scientists, 2012c. Site C0018. *In* Henry, P., Kanamatsu, T., Moe, K., and the Expedition 333 Scientists, *Proc. IODP*, 333: Washington, DC (Integrated Ocean Drilling Program Management International, Inc.). doi:10.2204/iodp.proc.333.103.2012

Fergusson, C.L., 2003. Provenance of Miocene–Pleistocene turbidite sands and sandstones, Nankai Trough, Ocean Drilling Program Leg 190. *In* Mikada, H., Moore, G.F., Taira, A., Becker, K., Moore, J.C., and Klaus, A. (Eds.), *Proc. ODP, Sci. Results,* 190/196: College Station, TX (Ocean Drilling Program), 1–28. doi:10.2973/odp.proc.sr.190196.205.2003

Gulick, S.P.S., Bangs, N.L.B., Moore, G.F., Ashi, J., Martin, K.M., Sawyer, D.S., Tobin, H.J., Kuramoto, S., and Taira, A., 2010. Rapid forearc basin uplift and megasplay fault development from 3D seismic images of Nankai Margin off Kii Peninsula, Japan. *Earth Planet. Sci. Lett.*, 300(1–2):55–62. doi:10.1016/j.epsl.2010.09.034

Hamamoto, H., Yamano, M., Goto, S., Kinoshita, M., Fujino, K., and Wang, K., 2011. Heat flow distribution and thermal structure of the Nankai subduction zone off the Kii Peninsula. *Geochem. Geophys. Geosyst.,* 12:Q0AD20. doi:10.1029/2011GC003623

Harris, R.N., Schmidt-Schierhorn, F., and Spinelli, G., 2011. Heat flow along the NanTroSEIZE transect: Results from IODP Expeditions 315 and 316 offshore the Kii Peninsula, Japan. *Geochem. Geophys. Geosyst.*, 12:Q0AD16. doi:10.1029/2011GC003593

Hayashida, A., Kamata, H., and Danhara, T., 1996. Correlation of widespread tephra deposits based on paleomagnetic directions: Link between a volcanic field and sedimentary sequences in Japan. *Quat. Int.*, 34–36:89–98. doi:10.1016/1040-6182(95)00072-0

Henry, P., Kanamatsu, T., and Moe, K.T., 2010. NanTroSEIZE Stage 2: Subduction inputs 2 and heat flow. *IODP Sci. Prosp.*, 333. doi:10.2204/iodp.sp.333.2010

Hyndman, R.D., Yamano, M., and Oleskevich, D.A., 1997. The seismogenic zone of subduction thrust faults. Island Arc, 6(3):244–260. doi:10.1111/j.1440-1738.1997.tb00175.x

Ike, T., Moore, G.F., Kuramoto, S., Park, J-O., Kaneda, Y., and Taira, A., 2008a. Tectonics and sedimentation around Kashinosaki Knoll: A subducting basement high in the eastern Nankai Trough. *Island Arc*, 17(3):358–375. doi:10.1111/j.1440-1738.2008.00625.x

Ike, T., Moore, G.F., Kuramoto, S., Park, J.-O., Kaneda, Y., and Taira, A., 2008b. Variations in sediment thickness and type along the northern Philippine Sea Plate at the Nankai Trough. *Island Arc*, 17(3):342–357. doi:10.1111/j.1440-1738.2008.00624.x

Ito, Y., Matsumoto, T., Kimura, H., Matsubayashi, H., Obara, K., and Sekiguchi, S., 2005. Spatial distribution of centroid moment tensor solutions for the 2004 off Kii peninsula earthquakes. *Earth Planets Space*, 57:351–356.

Kimura, G., Moore, G.F., Strasser, M., Screaton, E., Curewitz, D., Streiff, C., and Tobin, H., 2011. Spatial and temporal evolution of the megasplay fault in the Nankai Trough. *Geochem. Geophys. Geosyst.*, 12:Q0A008. doi:10.1029/2010GC003335

Kinoshita, M., Kanamatsu, T., Kawamura, K., Sibata, T., Hamamoto, H., and Fujino, K., 2008. Heat flow distribution on the floor of Nankai Trough off Kumano and implications for the geothermal regime of subducting sediments. *JAMSTEC Rep. Res. Dev.*, 8:13–28. http://docsrv.godac.jp/MSV2_DATA/23/JAM_RandD08_02.pdf

Kinoshita, M., Tobin, H., Ashi, J., Kimura, G., Lallemant, S., Screaton, E.J., Curewitz, D., Masago, H., Moe, K.T., and the Expedition 314/315/316 Scientists, 2009. *Proc. IODP*, 314/315/316: Washington, DC (Integrated Ocean Drilling Program Management International, Inc.). doi:10.2204/iodp.proc.314315316.2009

Kodaira, S., Nakanishi, A., Park, J.-O., Ito, A., Tsuru, T., and Kaneda, Y., 2003. Cyclic ridge subduction at an inter-plate locked zone off central Japan. *Geophys. Res. Lett.*, 30:1339–1342. doi:10.1029/2002GL016595

Kodaira, S., Takahashi, N., Nakanishi, A., Miura, S., and Kaneda, Y., 2000a. Subducted seamount imaged in the rupture zone of the 1946 Nankaido earthquake. *Science*, 289(5476):104–106. doi:10.1126/science.289.5476.104

Kodaira, S., Takahashi, N., Park, J.-O., Mochizuki, K., Shinohara, M., and Kimura, S., 2000b. Western Nankai Trough seismogenic zone: Results from a wide-angle ocean bottom seismic survey. *J. Geophys. Res.*, 105(B3):5887–5905. doi:10.1029/1999JB900394

Lallemand, S.E., Malavieille, J., and Calassou, S., 1992. Effects of oceanic ridge subduction on accretionary wedges: Experimental modeling and marine observations. *Tectonics*, 11(6):1301–1313. doi:10.1029/92TC00637

Le Pichon, X., Lallemant, S., Tokuyama, H., Thoué, F., Huchon, P., and Henry, P., 1996. Structure and evolution of the backstop in the Eastern Nankai Trough area (Japan): Implications for the soon-to-come Tokai earthquake. *Island Arc*, 5(4):440–454. doi:10.1111/j.1440-1738.1996.tb00164.x

Loveless, J.P., and Meade, B.J., 2010. Geodetic imaging of plate motions, slip rates, and partitioning of deformation in Japan. *J. Geophys. Res.*, 115:B02410. doi:10.1029/2008JB006248

Marcaillou, B., Henry, P., Kinoshita, M., Kanamatsu, T., Screaton, E.J., Daigle, H., Harcouët, V., et. al., 2012. Seismogenic zone temperatures and heat-flow anomalies in the To-nankai margin segment based on temperature data from IODP expedition 333 and thermal model. *Earth Planet. Sci. Lett.*, 349–350:171–185. doi:10.1016/j.epsl.2012.06.048

Mazzotti, S., Henry, P., and Le Pichon, X., 2001. Transient and permanent deformation of central Japan estimated by GPS2. Strain partitioning and arc-arc collision. *Earth Planet. Sci. Lett.*, 184:455–469.

Mazzotti, S., Lallemant, S.J., Henry, P., Le Pichon, X., Tokuyama, H., and Takahashi, N., 2002. Intraplate shortening and underthrusting of a large basement ridge in the eastern Nankai subduction zone. *Mar. Geol.*, 187(1–2):63–88. doi:10.1016/S0025-3227(02)00245-1

Moore, G.F., Bangs, N.L., Taira, A., Kuramoto, S., Pangborn, E., and Tobin, H.J., 2007. Three-dimensional splay fault geometry and implications for tsunami generation. *Science*, 318(5853):1128–1131. doi:10.1126/science.1147195

Moore, G.F., Park, J.-O., Bangs, N.L., Gulick, S.P., Tobin, H.J., Nakamura, Y., Sato, S., et al., 2009. Structural and seismic stratigraphic framework of the NanTroSEIZE Stage 1 transect. *In* Kinoshita, M., Tobin, H., Ashi, J., Kimura, G., Lallemant, S., Screaton, E.J., Curewitz, D., et al., *Proc. IODP*, 314/315/316: Washington, DC (Integrated Ocean Drilling Program Management International, Inc.). doi:10.2204/iodp.proc.314315316.102.2009

Moore, G.F., Taira, A., Klaus, A., et al., 2001. *Proc. ODP, Init. Repts.*, 190: College Station, TX (Ocean Drilling Program). doi:10.2973/odp.proc.ir.190.2001

Nagahashi, Y., and Satoguchi, Y., 2007. Stratigraphy of the Pliocene to lower Pleistocene marine formations in Japan on the basis of tephra beds correlation. *The Quaternary Research* [*Daiyonki Kenkyu*], 46(3):205–213. doi:10.4116/jaqua.46.205

Okino, K., Shimakawa, Y., and Nagaoka, S., 1994. Evolution of the Shikoku Basin. *J. Geomag. Geoelectr.*, 46(6):463–479.

Park, J.-O., Moore, G.F., Tsuru, T., Kodaira, S., and Kaneda, Y., 2004. A subducted oceanic ridge influencing the Nankai megathrust earthquake rupture. *Earth Planet. Sci. Lett.*, 217(1–2):77–84. doi:10.1016/S0012-821X(03)00553-3

Park, J.-O., Tsuru, T., Kaneda, Y., Kono, Y., Kodaira, S., Takahashi, N., and Kinoshita, H., 1999. A subducting seamount beneath the Nankai Accretionary Prism off Shikoku, southwestern Japan. *Geophys. Res. Lett.*, 26(7):931–934. doi:10.1029/1999GL900134

Park, J.-O., Tsuru, T., Kodaira, S., Cummins, P.R., and Kaneda, Y., 2002. Splay fault branching along the Nankai subduction zone. *Science*, 297(5584):1157–1160. doi:10.1126/science.1074111

Park, J.-O., Tsuru, T., No, T., Takizawa, K., Sato, S., and Kaneda, Y., 2008. High-resolution 3D seismic reflection survey and prestack depth imaging in the Nankai Trough off southeast Kii Peninsula. *Butsuri-Tansa [Geophys. Explor.]*, 61:231–241. (in Japanese, with abstract in English)

Saito, S., Underwood, M.B., Kubo, Y., and the Expedition 322 Scientists, 2010. *Proc. IODP*, 322: Washington, DC (Integrated Ocean Drilling Program Management International, Inc.). doi:10.2204/iodp.proc.322.2010

Satoguchi, Y., Higuchi, Y., and Kurokawa, K., 2005. Correlation of the Ohta tephra bed in the Tokai group with a tephra in the Miura group, central Japan. *Chishitsugaku Zasshi [J. Geol. Soc. Japan]*, 111(2):74–86.

Schacht, U., Wallmann, K., Kutterolf, S., and Schmidt, M., 2008. Volcanogenic sediment seawater interactions and the geochemistry of pore waters. *Chem. Geol.*, 249:321–338.

Screaton, E., Kimura, G., Curewitz, D., Moore, G., Chester, F., Fabbri, O., Fergusson, C., et al., 2009. Interactions between deformation and fluids in the frontal thrust region of the NanTroSEIZE transect offshore the Kii Peninsula, Japan: Results from IODP Expedition 316 Sites C0006 and C0007. *Geochem. Geophys. Geosyst.*, 10:Q0AD01. doi: 10.1029/2009GC002713

Seno, T., Stein, S., and Gripp, A.E., 1993. A model for the motion of the Philippine Sea Plate consistent with NUVEL-1 and geological data. *J. Geophys. Res.*, 98(B10):17941–17948. doi:10.1029/93JB00782

Spinelli, G.A., and Wang, K., 2008. Effects of fluid circulation in subduction crust on Nankai margin seismogenic zone temperatures. *Geology*, 36(11):887–890. doi:10.1130/G25145A.1

Spinelli, G.A., Mozley, P.S., Tobin, H.J., Underwood, M.B., Hoffman, N.W., and Bellew, G.M., 2007. Diagenesis, sediment strength, and pore collapse in sediment approaching the Nankai Trough subduction zone. *Geol. Soc. Am. Bull.*, 119(3–4):377–390.

Strasser, M., Henry, P., Kanamatsu, T., Thu, M.K., Moore, G.F., and the IODP Expedition 333 Scientists, 2012. Scientific drilling of mass-transport deposits in the Nankai accretionary wedge: First results from IODP Expedition 333. *In* Yamada, Y., Kawamura, K., Ikehara, K., Ogawa, Y., Urgeles, R., Mosher, D., Chaytor, J., and Strasser, M. (Eds.), *Submarine Mass Movements and Their Consequences, Adv. Nat. Technol. Hazard Res.*, 31:671–681. doi:10.1007/978-94-007-2162-3_60

Strasser, M., Moore, G.F., Kimura, G., Kitamura, Y., Kopf, A.J., Lallemant, S., Park, J.-O., Screaton, E.J., Su, X., Underwood, M.B., and Zhao, X., 2009. Origin and evolution of a splay fault in the Nankai accretionary wedge. *Nat. Geosci.*, 2:648–652. doi:10.1038/ngeo609

Strasser, M., Moore, G.F., Kimura, G., Kopf, A., Underwood, M., Guo, J., and Screaton, E.J., 2011. Slumping and mass transport deposition in the Nankai fore arc: Evidence from IODP drilling and 3-D reflection seismic data. *Geochem. Geophys. Geosyst.*, 12:Q0AD13. doi:10.1029/2010GC003431

Tobin, H.J., and Kinoshita, M., 2006a. Investigations of seismogenesis at the Nankai Trough, Japan. *IODP Sci. Prosp.*, NanTroSEIZE Stage 1. doi:10.2204/iodp.sp.nantroseize1.2006

Tobin, H.J., and Kinoshita, M., 2006b. NanTroSEIZE: The IODP Nankai Trough Seismogenic Zone Experiment. *Sci. Drill.*, 2:23–27. doi:10.2204/iodp.sd.2.06.2006

Tobin, H., Kinoshita, M., Ashi, J., Lallemant, S., Kimura, G., Screaton, E.J., Moe, K.T., Masago, H., Curewitz, D., and the Expedition 314/315/316 Scientists, 2009. NanTroSEIZE Stage 1 expeditions: Introduction and synthesis of key results. *In* Kinoshita, M., Tobin, H., Ashi, J., Kimura, G., Lallemant, S., Screaton, E.J., Curewitz, D., Masago, H., Moe, K.T., and the Expedition 314/315/316 Scientists, *Proc. IODP*, 314/315/316: Washington, DC (Integrated Ocean Drilling Program Management International, Inc.). doi:10.2204/iodp.proc.314315316.101.2009

Underwood, M.B., 2007. Sediment inputs to subduction zones: Why lithostratigraphy and clay mineralogy matter. *In* Dixon, T., and Moore, J.C. (Eds.), *The Seismogenic Zone of Subduction Thrust Faults:* New York (Columbia University Press), 42–85.

Underwood, M.B., Saito, S., Kubo, Y., and the Expedition 322 Scientists, 2010. Expedition 322 summary. *In* Saito, S., Underwood, M.B., Kubo, Y., and the Expedition 322 Scientists, *Proc. IODP*, 322: Washington, DC (Integrated Ocean Drilling Program Management International, Inc.). doi:10.2204/iodp.proc.322.101.2010

White, R., Spinelli, G.A., Mozley, P.S., and Dunbar, N.W., 2011. Importance of volcanic glass alteration to sediment stabilization: Offshore Japan. *Sedimentology*, 58(5):1138–1154. doi:10.1111/j.1365-3091.2010.01198.x

Authors

Pierre Henry, Centre Européen de Recherche et d'Enseignement en Géosciences de l'Environnement, Aix-Marseille Université et CNRS, Europôle de l'Arbois, 13545 Aix en Provence Cedex 04, France, e-mail: henry@cerege.fr

Toshiya Kanamatsu, Institute for Research on Earth Evolution, Japan Agency for Marine-Earth Science and Technology, 2-15 Natsushima-cho, Yokosuka, Kanagawa 237-0061, Japan

Kyaw Thu Moe, Center for Deep Earth Exploration, Japan Agency for Marine-Earth Science and Technology, 3173-25 Showa-machi, Kanazawa-ku, Yokohama, Kanagawa, 236-0001, Japan

Michael Strasser, ETH Zürich, Geologisches Institut, Sonneggstrasse 5, 8092 Zürich, Switzerland

and the IODP Expedition 333 Scientific Party